

Blind Beam-Hardening Correction from Poisson Measurements[†]

Aleksandar Dogandžić

Electrical and Computer Engineering
IOWA STATE UNIVERSITY

[†] joint work with Renliang Gu, Ph.D. student

supported by 

Terminology and Notation I

- “ \succeq ” is the elementwise version of “ \geq ”;
 - B1 spline means B-spline of order 1,
 - For a vector $a = [a_1, \dots, a_N]^T \in \mathbb{R}^N$, define
 - nonnegativity indicator function

$$\mathbb{I}_{[0,+\infty)}(a) \triangleq \begin{cases} 0, & a \geq 0 \\ +\infty, & \text{o.w.} \end{cases}$$

- elementwise logarithm

$$[\ln_o(a)]_i = \ln a_i, \quad \forall i.$$

Terminology and Notation II

- $\mathfrak{l}^L(s)$ is the *Laplace transform* of $\mathfrak{l}(k)$:

$$\iota^L(s) \triangleq \int \iota(\kappa) e^{-s\kappa} d\kappa,$$

- Laplace transform with vector argument:

$$b_o^L(s) = b_o^L \begin{pmatrix} s_1 \\ s_2 \\ \vdots \\ s_N \end{pmatrix} = \begin{bmatrix} b^L(s_1) \\ b^L(s_2) \\ \vdots \\ b^L(s_N) \end{bmatrix}.$$

X-ray CT

An X-ray computed tomography (CT) scan consists of multiple projections with the beam intensity measured by multiple detectors.

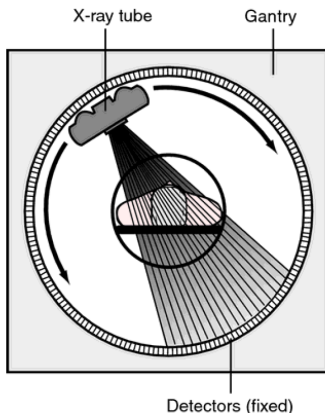


Figure 1: Fan-beam CT system.

Parallel- and Fan-Beam Systems

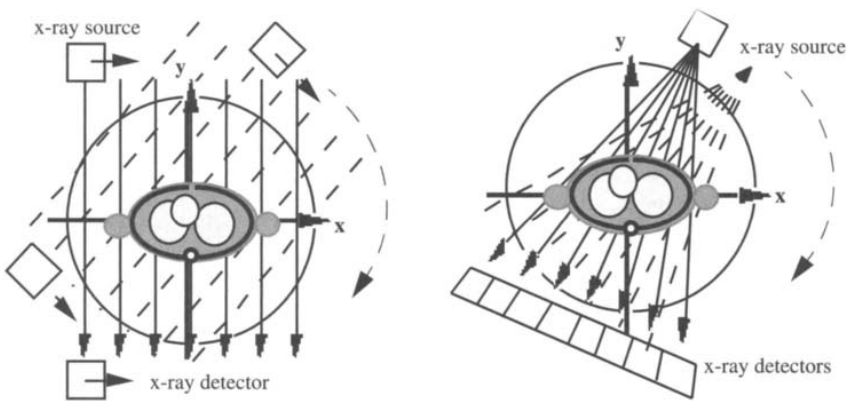
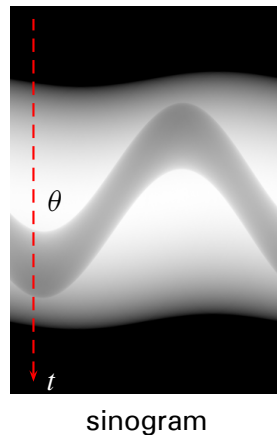
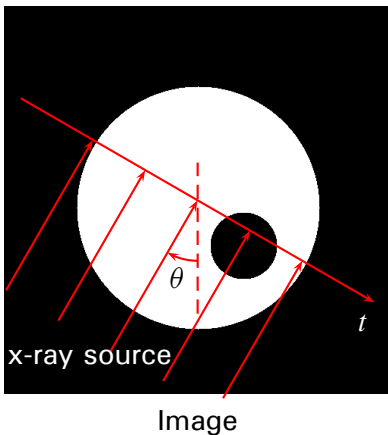


Figure 2: (Left) first-generation scanner, uses **source translation and rotation** and a single detector to collect a complete set of 1D parallel projections and (right) the current generation scanner, uses a fan x-ray beam and an array of detectors, requires **rotation only**.

Introduction to CT Imaging (Parallel Beam)

A detector array is deployed parallel to the t axis and rotates against the X-ray source collecting projections. Sinogram is the set of collected projections as a function of angle at which they are taken.



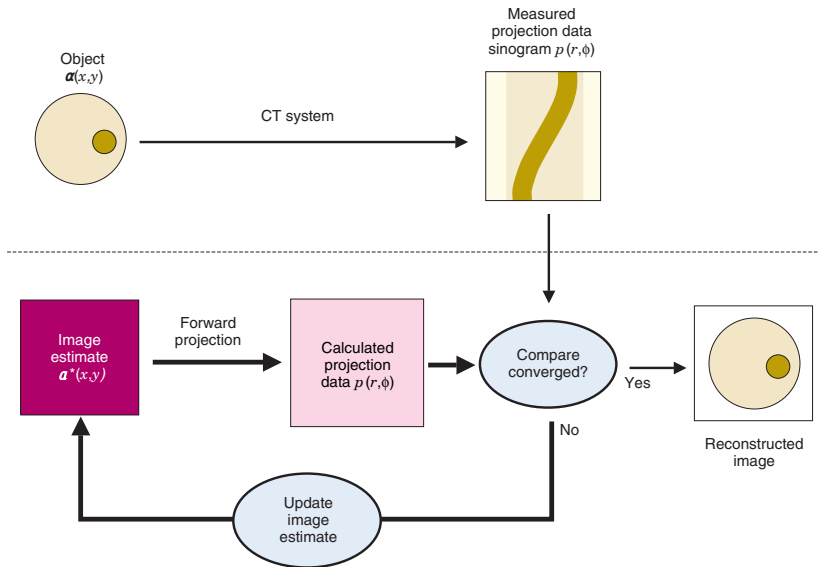
X-ray CT Scans: Fan Bean



CT image reconstruction problem:

Determine unknown attenuation map a given sinogram data y using system matrix Φ .

Iterative Reconstruction



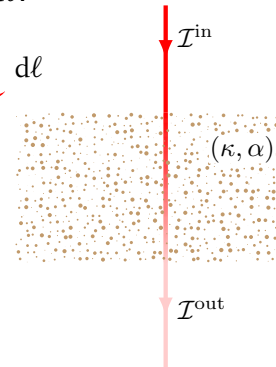
Exponential Law of Absorption

The fraction $d\mathcal{I}/\mathcal{I}$ of plane-wave intensity lost in traversing an infinitesimal thickness $d\ell$ at Cartesian coordinates (x, y) is proportional to $d\ell$:

$$\frac{d\mathcal{I}}{\mathcal{I}} = - \underbrace{\mu(x, y, \varepsilon)}_{\text{attenuation}} d\ell = - \underbrace{\kappa(\varepsilon) \alpha(x, y)}_{\text{separable}} d\ell$$

where ε is **photon energy** and

- $\kappa(\varepsilon) \geq 0$ is the **mass attenuation function** of the material and
- $\alpha(x, y) \geq 0$ is the **density map** of the inspected object.



To obtain the intensity decrease along a straight-line path $\ell = \ell(x, y)$, integrate along ℓ and over ε . The underlying measurement model is **nonlinear**.

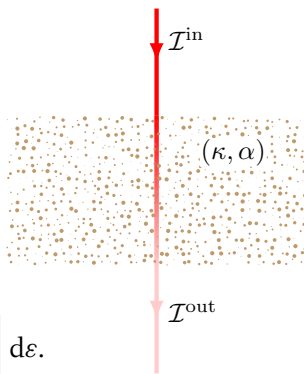
Polychromatic X-ray CT Model

- Incident energy \mathcal{I}^{in} spreads along photon energy ε with density $\iota(\varepsilon)$:

$$\int \iota(\varepsilon) d\varepsilon = \mathcal{I}^{\text{in}}.$$

- Noiseless energy measurement obtained upon traversing a straight line $\ell = \ell(x, y)$ through an object composed of a single material:

$$\mathcal{I}^{\text{out}} = \int \iota(\varepsilon) \exp \left[-\kappa(\varepsilon) \int_{\ell} \alpha(x, y) d\ell \right] d\varepsilon.$$



Linear Reconstruction Artifacts

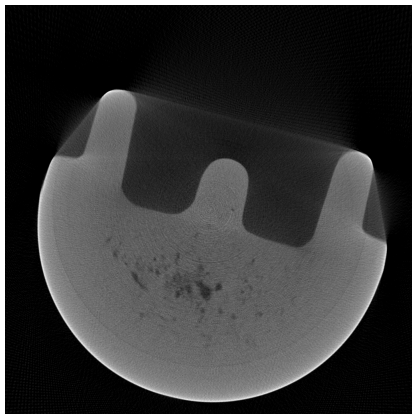


Figure 3: FBP reconstruction of an industrial object.

Note the cupping and streaking artifacts of the linear filtered backprojection (FBP) reconstruction, applied to $\ln \mathcal{I}^{\text{out}}$.

Problem Formulation and Goal

Assume that both

- o the incident spectrum $\iota(\varepsilon)$ of X-ray source and
- o mass attenuation function $\kappa(\varepsilon)$ of the object

are **unknown**.

Problem Formulation and Goal

Assume that both

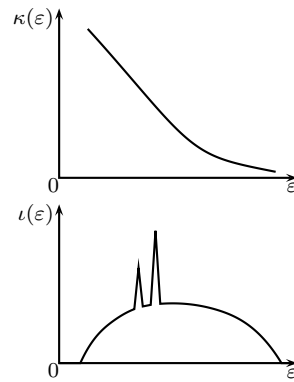
- o the incident spectrum $\iota(\varepsilon)$ of X-ray source and
- o mass attenuation function $\kappa(\varepsilon)$ of the object

are **unknown**.

Goal: Estimate the density map $\alpha(x, y)$.

Polychromatic X-ray CT Model Using Mass-Attenuation Spectrum

Mass attenuation $\kappa(\varepsilon)$ and incident spectrum density $\iota(\varepsilon)$ are both functions of ε .



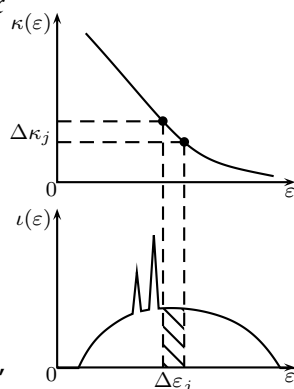
Polychromatic X-ray CT Model Using Mass-Attenuation Spectrum

Mass attenuation $\kappa(\varepsilon)$ and incident spectrum density $\iota(\varepsilon)$ are both functions of ε .

Idea. Write the model as integrals of κ rather than ε :

$$\mathcal{I}^{\text{in}} = \int \iota(\kappa) d\kappa = \iota^L(0)$$

$$\begin{aligned}\mathcal{I}^{\text{out}} &= \int \iota(\kappa) \exp\left[-\kappa \int_{\ell} \alpha(x, y) d\ell\right] d\kappa \\ &= \iota^L\left(\int_{\ell} \alpha(x, y) d\ell\right).\end{aligned}$$



☞ Need to estimate **one** function, $\iota(\kappa)$, rather than **two**, $\iota(\varepsilon)$ and $\kappa(\varepsilon)$!

Mass-Attenuation Spectrum

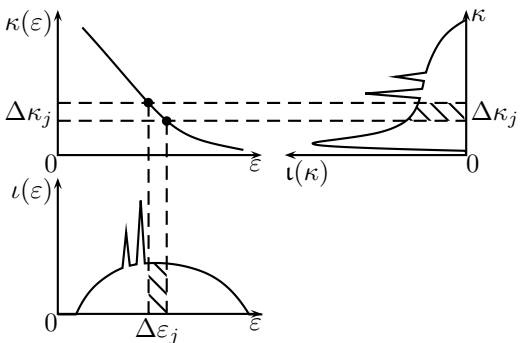
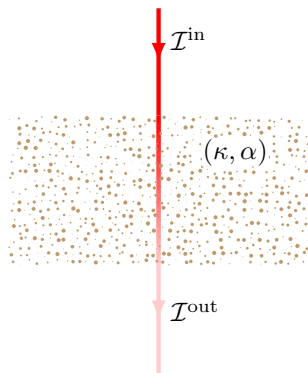


Figure 4: Relation between mass attenuation κ , incident spectrum ι , photon energy ε , and **mass attenuation spectrum** $\iota(\kappa)$.

Noiseless Polychromatic X-ray CT Model Using Mass-Attenuation Spectrum $\iota(\kappa)$: Summary

$$\begin{aligned}\mathcal{I}^{\text{in}} &= \iota^L(0) \\ \mathcal{I}^{\text{out}} &= \iota^L\left(\int_{\ell} \alpha(x, y) d\ell\right)\end{aligned}$$



▶ more

Mass-Attenuation Spectrum and Linearization Function

- For $s > 0$, the function

$$\iota^L(s) = \int_0^{+\infty} \iota(\kappa) e^{-s\kappa} d\kappa$$

is an invertible decreasing function of s .

Mass-Attenuation Spectrum and Linearization Function

- For $s > 0$, the function

$$\iota^L(s) = \int_0^{+\infty} \iota(\kappa) e^{-s\kappa} d\kappa$$

is an invertible decreasing function of s .

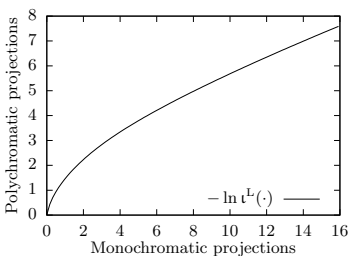
- $(\iota^L)^{-1}$ converts the noiseless measurement

$$\mathcal{I}^{\text{out}} = \iota^L \left(\int_{\ell} \alpha(x, y) d\ell \right)$$

into a linear noiseless “measurement” $\int_{\ell} \alpha(x, y) d\ell$.

Mass-Attenuation Spectrum and Linearization Function

The $(\iota^L)^{-1} \circ \exp(-\cdot)$ mapping corresponds to the *linearization function* in (Herman 1979) and converts $\ln \mathcal{I}^{\text{out}}$ into a linear noiseless “measurement” $\int_{\ell} \alpha(x, y) d\ell$.



- The standard FBP method fits a linear model to log of the energy measurements
 - for monochromatic X-ray source, $-\ln \mathcal{I}^{\text{out}}$ is an affine function of $\int_{\ell} \alpha(x, y) d\ell$.

Basis-function expansion of mass-attenuation spectrum $\iota(\kappa) = \mathbf{b}(\kappa)\mathcal{I}$

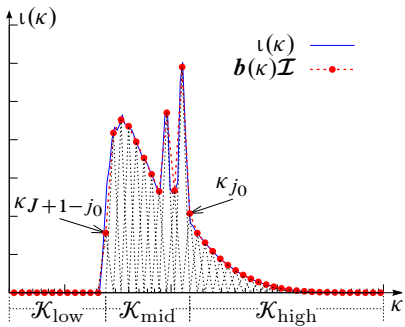


Figure 5: B1-spline expansion $\iota(\kappa) = \mathbf{b}(\kappa)\mathcal{I}$, where the B1-spline basis is $\underbrace{\mathbf{b}(\kappa)}_{1 \times J} = [b_1(\kappa), b_2(\kappa), \dots, b_J(\kappa)]$. $\iota(\kappa) \geq 0$ implies $\mathcal{I} \succeq \mathbf{0}$.

B1-Spline Basis Functions

Select spline knots from a growing geometric series with common ratio

$$q > 1$$

which yields the B1-spline basis functions:

$$b_j(\kappa) = \begin{cases} \frac{\kappa - q^{j-1}\kappa_0}{(q-1)q^{j-1}\kappa_0}, & q^{j-1}\kappa_0 \leq \kappa < q^j\kappa_0 \\ \frac{-\kappa + q^{j+1}\kappa_0}{(q-1)q^j\kappa_0}, & q^j\kappa_0 \leq \kappa < q^{j+1}\kappa_0 \\ 0, & \text{otherwise} \end{cases}$$

where the j th basis function can be obtained by q -scaling the $(j-1)$ th basis function:

$$b_j(\kappa) = b_{j+1}(q\kappa).$$

Comments

- The geometric-series knots have a wide span, from κ_0 to $q^{J+1}\kappa_0$, and compensate larger κ with a “geometrically” wider integral range, which results in an effective approximation of the noiseless measurements.

Comments

- The geometric-series knots have a wide span, from κ_0 to $q^{J+1}\kappa_0$, and compensate larger κ with a “geometrically” wider integral range, which results in an effective approximation of the noiseless measurements.
- The common ratio q determines the resolution of the B1-spline approximation.

Comments

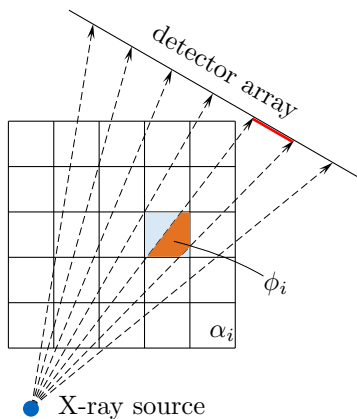
- The geometric-series knots have a wide span, from κ_0 to $q^{J+1}\kappa_0$, and compensate larger κ with a “geometrically” wider integral range, which results in an effective approximation of the noiseless measurements.
- The common ratio q determines the resolution of the B1-spline approximation.
- In summary, the following three tuning constants:

$$(q, \kappa_0, J)$$

define our B1-spline basis functions $b(\kappa)$.

Discretization of $\alpha(x, y)$

- $\alpha \succeq \mathbf{0}$ is a $p \times 1$ vector representing the 2D image that we wish to reconstruct and
- $\phi \succeq \mathbf{0}$ is a $p \times 1$ vector of known weights quantifying how much each element of α contributes to the X-ray attenuation on the straight-line path ℓ .



$$\int_{\ell} \alpha(x, y) \, d\ell \approx \phi^T \alpha.$$

Shift Ambiguity of the Mass-Attenuation Spectrum

By noting

$$b_j(\kappa) = b_{j+1}(q\kappa).$$

and the κ -scaling property of the Laplace transform,

$$b_j(q\kappa) \xrightarrow{\mathcal{L}} \frac{1}{q} b_j^L\left(\frac{s}{q}\right)$$

we conclude that selecting q times narrower basis functions

$$\mathbf{b}(q\kappa) = [b_0(q\kappa), b_1(q\kappa), \dots, b_{J-1}(q\kappa)]$$

and q times larger density map and spectral parameters ($q\alpha$ and $q\mathcal{I}$) yields the same mean output photon energy.

Proof

Mean output photon energy:

$$\begin{aligned}\mathcal{I}^{\text{out}}(\alpha, \mathcal{I}; \mathbf{b}(\kappa)) &= b_o^L(\Phi\alpha)\mathcal{I} \\ \mathcal{I}^{\text{out}}(q\alpha, q\mathcal{I}; \mathbf{b}(q\kappa)) &= \frac{1}{q}b_o^L\left(\frac{\Phi q\alpha}{q}\right)q\mathcal{I}\end{aligned}$$

The right-hand sides are identical!

Shift Ambiguity of the Mass-Attenuation Spectrum

$$\mathcal{I}^{\text{out}}(\alpha, [0, \mathcal{I}_2, \dots, \mathcal{I}_J]^T) = \mathcal{I}^{\text{out}}(q\alpha, q[\mathcal{I}_2, \dots, \mathcal{I}_J, 0]^T).$$

This *shift ambiguity* of the mass-attenuation spectrum allows us to rearrange leading or trailing zeros in the mass-attenuation coefficient vector \mathcal{I} and position the central nonzero part of \mathcal{I} .

Multiple Measurements and Projection Matrix

- Denote by N the total number of measurements from all projections collected at the detector array.
- For the n th measurement, define its discretized line integral as $\phi_n^T \alpha$.
- Stacking all N such integrals into a vector yields

$$\underbrace{\Phi \alpha}_{\text{monochromatic projection of } \alpha}$$

where

$$\underbrace{\Phi}_{\text{projection matrix}} = \begin{bmatrix} \phi_1^T \\ \phi_2^T \\ \vdots \\ \phi_N^T \end{bmatrix}_{N \times p} .$$

Noiseless Measurement Model

The $N \times 1$ vector of noiseless measurements is

$$\mathcal{I}^{\text{out}}(\boldsymbol{\alpha}, \mathcal{I}) = \underbrace{\mathbf{b}_o^L(\Phi\boldsymbol{\alpha})}_{\substack{\text{output} \\ \text{basis-function} \\ \text{matrix}}} \quad \mathcal{I}$$

where

$$\mathbf{b}_o^L(s) = \begin{bmatrix} \mathbf{b}^L(s_1) \\ \mathbf{b}^L(s_2) \\ \vdots \\ \mathbf{b}^L(s_N) \end{bmatrix}$$

and $s = \Phi\boldsymbol{\alpha}$ is the monochromatic projection.

Noise Model

- Assume noisy Poisson-distributed measurements $\mathcal{E} = (\mathcal{E}_n)_{n=1}^N$, with the negative log-likelihood (NLL) function

$$\mathcal{L}(\Phi\alpha, \mathcal{I})$$

where

$$\mathcal{L}(s, \mathcal{I}) = \mathbf{1}^T [\mathbf{b}_o^L(s)\mathcal{I} - \mathcal{E}] - \mathcal{E}^T \left\{ \ln_o [\mathbf{b}_o^L(s)\mathcal{I}] - \ln_o \mathcal{E} \right\}.$$

- The Poisson model is a good approximation for the more precise compound-Poisson distribution (Xu and Tsui 2014; Lasio *et al.* 2007).

NLL of \mathcal{I}

Define $A = \mathbf{b}_o^L(\Phi\alpha)$.

The NLL of \mathcal{I} for known α reduces to the NLL for Poisson generalized linear model (GLM)[‡] with identity link and design matrix A :

$$\mathcal{L}_A(\mathcal{I}) = \mathbf{1}^T(A\mathcal{I} - \mathcal{E}) - \mathcal{E}^T [\ln_o(A\mathcal{I}) - \ln_o \mathcal{E}].$$

[‡]See (McCullagh and Nelder 1989) for introduction to GLMs.

NLL of α

The NLL of α for fixed $\iota(\kappa)$ is also a Poisson GLM:

$$\mathcal{L}_\iota(\alpha) = \mathbf{1}^T [\iota_o^L(\Phi\alpha) - \mathcal{E}] - \mathcal{E}^T \left\{ \ln_o [\iota_o^L(\Phi\alpha)] - \ln_o \mathcal{E} \right\}$$

with the link function equal to the inverse of $\iota^L(\cdot)$. Since $\iota(\kappa)$ is known, we do not need its basis-function expansion.

NLL of α

The NLL of α for fixed $\iota(\kappa)$ is also a Poisson GLM:

$$\mathcal{L}_\iota(\alpha) = \mathbf{1}^T [\iota_o^L(\Phi\alpha) - \mathcal{E}] - \mathcal{E}^T \left\{ \ln_o [\iota_o^L(\Phi\alpha)] - \ln_o \mathcal{E} \right\}$$

with the link function equal to the inverse of $\iota^L(\cdot)$. Since $\iota(\kappa)$ is known, we do not need its basis-function expansion.



$\mathcal{L}_\iota(\alpha)$ is convex, under conditions that we established in (G. and D. 2016)!

Regularized NLL Minimization

$$\min_{\alpha, \mathcal{I}} \underbrace{\mathcal{L}(\Phi\alpha, \mathcal{I}) + ur(\alpha) + \mathbb{I}_{[0,+\infty)}(\mathcal{I})}_{\triangleq f(\alpha, \mathcal{I})}$$

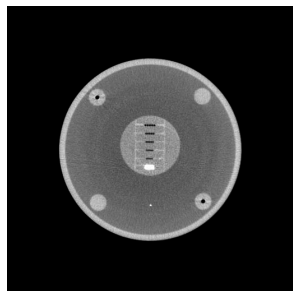
where $u > 0$ is a scalar tuning constant and $r(\alpha)$ is the density-map regularization term:

$$r(\alpha) = \|\psi(\alpha)\|_1 + \mathbb{I}_{[0,+\infty)}(\alpha).$$

Here, $\psi(\alpha) = (\psi_i(\alpha))_{i=1}^p$, where

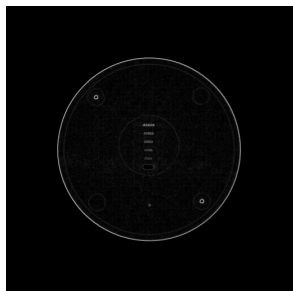
- $\psi_i(\alpha) = \sqrt{\sum_{j \in \mathcal{N}_i} (\alpha_i - \alpha_j)^2}$ is the gradient map,
- \mathcal{N}_i is the index set of neighbors of α_i in an appropriate 2D arrangement.

TV Sparsifying Transform



p pixels

\leftrightarrow
grad. map $\psi_i(\alpha)$



significant coeffs $\ll p$

Goal and Minimization Approach

Goal: Estimate the density-map and mass-attenuation spectrum parameters

$$(\alpha, \mathcal{I})$$

by minimizing the penalized NLL $f(\alpha, \mathcal{I})$.

Approach: A block coordinate-descent that uses

- Nesterov's proximal-gradient (NPG) (Nesterov 2013) and
- limited-memory Broyden-Fletcher-Goldfarb-Shanno with box constraints (L-BFGS-B) (Byrd *et al.* 1995)

methods to update estimates of the **density map** and **mass-attenuation spectrum** parameters.

We refer to this iteration as NPG-BFGS algorithm.

Iteration i of NPG-BFGS

Alternate between ① and ②:

- ① **Update α using NPG.** Set the mass-attenuation spectrum $\iota(\kappa) = b(\kappa)\mathcal{I}^{(i-1)}$ and descend the objective function $f(\alpha, \mathcal{I}^{(i-1)}) = \mathcal{L}_1(\alpha) + ur(\alpha)$ by applying an NPG step for α , which yields $\alpha^{(i)}$:

$$f(\alpha^{(i)}, \mathcal{I}^{(i-1)}) \leq f(\alpha^{(i-1)}, \mathcal{I}^{(i-1)}).$$

- ② **Update \mathcal{I} using BFGS.** Set $A = b_o^L(\Phi\alpha^{(i)})$ and minimize $f(\alpha^{(i)}, \mathcal{I})$:

$$\mathcal{I}^{(i)} = \arg \min_{\mathcal{I} \succeq 0} \mathcal{L}_A(\mathcal{I})$$

using the inner L-BFGS-B iteration.

1 Update α : NPG Step

Set $\iota(\kappa) = b(\kappa)\mathcal{I}^{(i-1)}$ and compute the new iterate of α as

$$\alpha^{(i)} = \arg \min_{\alpha} (\alpha - \bar{\alpha}^{(i)})^T \nabla \mathcal{L}_\iota(\bar{\alpha}^{(i)}) + \frac{1}{2\beta^{(i)}} \|\alpha - \bar{\alpha}^{(i)}\|_2^2 + ur(\alpha)$$

where $\beta^{(i)} > 0$ is a step size,

$$\bar{\alpha}^{(i)} = \alpha^{(i-1)} + \frac{\theta^{(i-1)} - 1}{\theta^{(i)}} (\alpha^{(i-1)} - \alpha^{(i-2)}) \quad \text{Nesterov accel.}$$

$$\theta^{(i)} = \frac{1}{2} \left[1 + \sqrt{1 + 4(\theta^{(i-1)})^2} \right]$$

and the minimization is computed using an inner iteration that employs the total-variation (TV)-based denoising method in (Beck and Teboulle 2009, Sec. IV).

Comments

- The optimization task in Step ① is a proximal-gradient (PG) step:

$$\boldsymbol{\alpha}^{(i)} = \text{prox}_{\beta^{(i)} \mathcal{U} \mathcal{R}} \left(\bar{\boldsymbol{\alpha}}^{(i)} - \beta^{(i)} \nabla \mathcal{L}_1(\bar{\boldsymbol{\alpha}}^{(i)}) \right);$$

- If we *do not* apply the Nesterov's acceleration and use only the PG step to update the density-map iterates $\boldsymbol{\alpha}$, i.e., $\bar{\boldsymbol{\alpha}}^{(i)} = \boldsymbol{\alpha}^{(i-1)}$, then the corresponding iteration is the *PG-BFGS algorithm*;
- We select the step size $\beta^{(i)}$ adaptively to account for varying local Lipschitz constants of the objective function and restart the Nesterov acceleration by $\theta^{(i)} = 0$ when the objective function $f(\boldsymbol{\alpha}, \mathcal{I})$ is not decreasing (O'Donoghue and Candès 2015).

2 Update \mathcal{I} : L-BFGS-B

- Broyden-Fletcher-Goldfarb-Shanno (BFGS) iteration used to update iterates of \mathcal{I} is a state-of-the-art *quasi-Newton method* (Thisted 1989, Sec. 4.3.3.4).
- box constraints in the L-BFGS-B variant impose the nonnegativity

$$\mathcal{I} \succeq \mathbf{0}.$$

▶ more

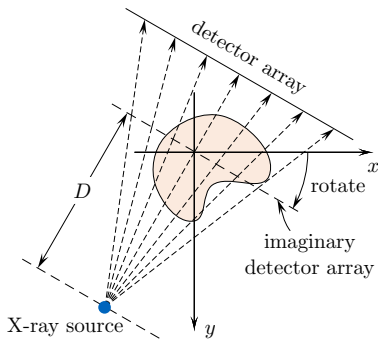
Numerical Examples

B1-spline constants set to satisfy

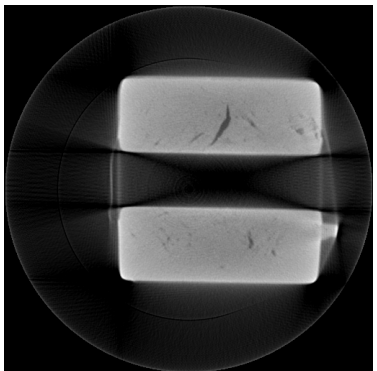
$$\begin{aligned} J &= 20, && \text{\# basis functions} \\ q^J &= 10^3, && \text{span} \\ \kappa_0 q^{\lceil 0.5(J+1) \rceil} &= 1, && \text{centering} \end{aligned}$$

Real X-ray CT Example I

- 360 equi-spaced fan-beam projections with 1° spacing,
- X-ray source to rotation center is $3492 \times$ detector size,
- measurement array size of 694 elements,
- projection matrix Φ constructed directly on GPU,



yielding a nonlinear estimation problem with $N = 694 \times 360$ measurements and an 512×512 image to reconstruct.
Implementation available at github.com/isucsp/imgRecSrc.



(a) FBP

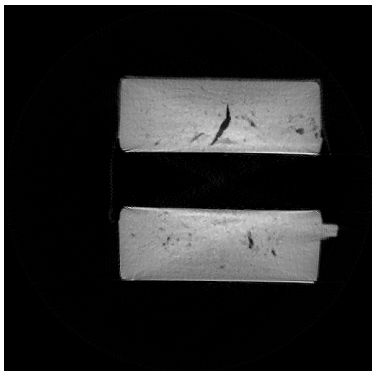
(b) NPG-BFGS ($u = 10^{-5}$)

Figure 6: Real X-ray CT: Full projections.

Comments I

Our reconstruction eliminates

- the streaking artifacts across the air around the object,
- the cupping artifacts with high intensity along the border.

The regularization constant μ has been tuned for good reconstruction performance.

Comments II

- The slight non-uniformity of the reconstructed density map in Fig. 6b may be due to
 - detector saturation that leads to measurement truncation,
 - scattering,
 - noise-model mismatch, or
 - the bowtie filter applied to the X-ray source.
- We leave further verification of causes and potential correction of this problem to future work and note that this issue does not occur in the simulated-data examples that we constructed.

Inverse Linearization Function Estimate

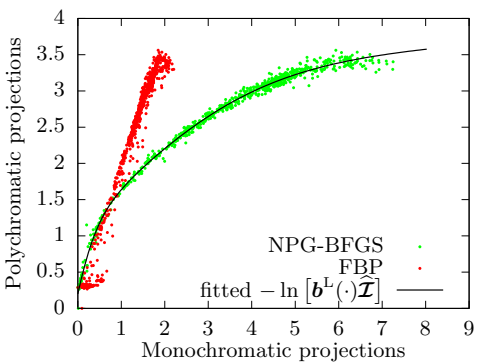


Figure 7: The polychromatic measurements as function of the monochromatic projections and its corresponding fitted curve.

Observe the biased residual for FBP, the unbiased residual for NPG-BFGS and its increasing variance.

Real X-ray CT Example II

- 360 and 120 equi-spaced fan-beam projections,
- X-ray source to rotation center is 8696 times of a single detector size,
- measurement array size of 1380 elements,
- projection matrix Φ constructed on **GPU** with full circular mask.

yielding a nonlinear estimation problem with $N = 1380 \times 360$ measurements and an 1024×1024 image to reconstruct.

We employ same convergence constants as in the previous example.

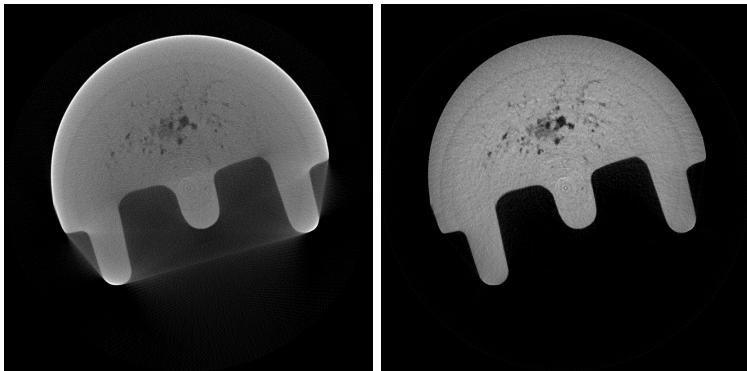


Figure 8: Reconstructions from 360 fan-beam projections with 1° spacing.

Figure 9: Estimated α and $-\ln [b^L(\cdot)\mathcal{I}]$ from 360 fan-beam projections.

Inverse Linearization Function Estimate

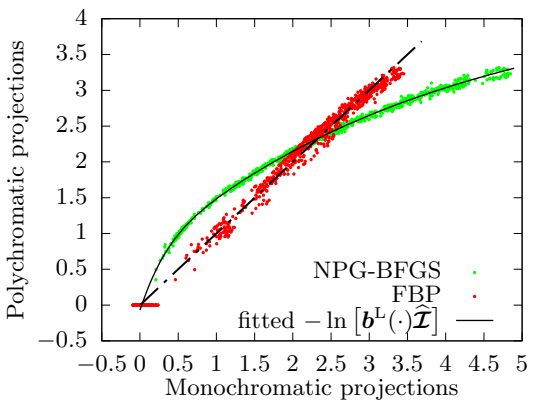


Figure 10: The polychromatic measurements as function of the monochromatic projections and its corresponding fitted curve.

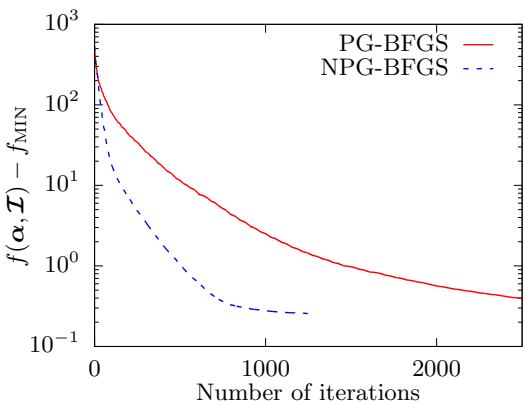
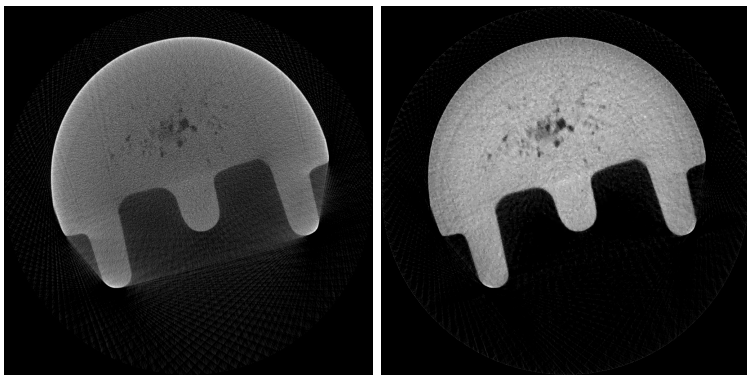


Figure 11: The objective function as a function of iteration index.



(a) FBP

(b) NPG-BFGS ($u = 10^{-5}$)

Figure 12: Reconstructions from 120 fan-beam projections with 3° spacing.

Observe aliasing artifacts in the FBP reconstruction.

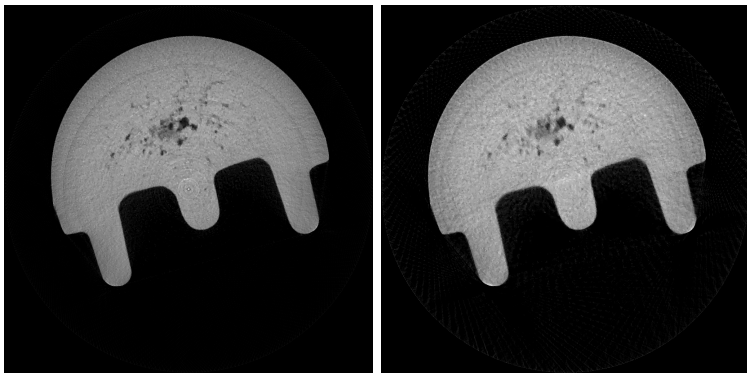


Figure 13: NPG-BFGS ($u = 10^{-5}$) reconstructions from fan-beam projections.

The reconstructed density maps are uniform, except the defect region.

Biconvexity, KL Property, and Convergence

- Under certain condition,
 - $\mathcal{L}(\Phi\alpha, \mathcal{I})$ is biconvex with respect to α and \mathcal{I} .
 - our objective function $f(\alpha, \mathcal{I})$ satisfies the Kurdyka-Łojasiewicz (KL) inequality.
- The above facts can be used to establish the local convergence for alternating proximal minimization methods (Attouch *et al.* 2010; Xu and Yin 2013)
 - e.g., PG-BFGS,
 - not NPG-BFGS.

See (G. and D. 2016; G. and D. 2015).

Conclusion

Developed a blind method for sparse density-map image reconstruction from polychromatic X-ray CT measurements in Poisson noise.

Future Work

- Apply to more real X-ray CT data sets to test and potentially improve our proposed algorithm,
- Generalize our polychromatic signal model to handle multiple materials and develop corresponding reconstruction schemes.

Publications

- R. G. and A. D., "Blind X-ray CT image reconstruction from polychromatic Poisson measurements", *IEEE Trans. Comput. Imag.*, vol. 2, no. 2, pp. 150–165, 2016. doi: [10.1109/tci.2016.2523431](https://doi.org/10.1109/tci.2016.2523431).
- R. G. and A. D. (Sep. 2015), Polychromatic X-ray CT image reconstruction and mass-attenuation spectrum estimation, arXiv: [1509.02193 \[stat.ME\]](https://arxiv.org/abs/1509.02193).

References I

-  H. Attouch, J. Bolte, P. Redont, and A. Soubeyran, "Proximal alternating minimization and projection methods for nonconvex problems: An approach based on the Kurdyka-Łojasiewicz inequality", *Math. Oper. Res.*, vol. 35, no. 2, pp. 438–457, May 2010.
-  A. Beck and M. Teboulle, "Fast gradient-based algorithms for constrained total variation image denoising and deblurring problems", *IEEE Trans. Image Process.*, vol. 18, no. 11, pp. 2419–2434, 2009.
-  R. H. Byrd, P. Lu, J. Nocedal, and C. Zhu, "A limited memory algorithm for bound constrained optimization", *SIAM J. Sci. Comput.*, vol. 16, no. 5, pp. 1190–1208, 1995.
-  R. G. and A. D. (Sep. 2015), Polychromatic X-ray CT image reconstruction and mass-attenuation spectrum estimation, [arXiv: 1509.02193 \[stat.ME\]](https://arxiv.org/abs/1509.02193).
-  R. G. and A. D., "Blind X-ray CT image reconstruction from polychromatic Poisson measurements", *IEEE Trans. Comput. Imag.*, vol. 2, no. 2, pp. 150–165, 2016.
-  G. T. Herman, "Correction for beam hardening in computed tomography", *Phys. Med. Biol.*, vol. 24, no. 1, pp. 81–106, 1979.

References II

-  A. C. Kak and M. Slaney, *Principles of Computerized Tomographic Imaging*. New York: IEEE Press, 1988.
-  G. M. Lasio, B. R. Whiting, and J. F. Williamson, "Statistical reconstruction for X-ray computed tomography using energy-integrating detectors", *Phys. Med. Biol.*, vol. 52, no. 8, p. 2247, 2007.
-  P. McCullagh and J. Nelder, *Generalized Linear Models*, 2nd ed. New York: Chapman & Hall, 1989.
-  Y. Nesterov, "Gradient methods for minimizing composite functions", *Math. Program.*, vol. 140, no. 1, pp. 125–161, 2013.
-  B. O'Donoghue and E. Candès, "Adaptive restart for accelerated gradient schemes", *Found. Comput. Math.*, vol. 15, no. 3, pp. 715–732, 2015.
-  R. A. Thisted, *Elements of Statistical Computing*. New York: Chapman & Hall, 1989.
-  J. Xu and B. M. Tsui, "Quantifying the importance of the statistical assumption in statistical X-ray CT image reconstruction", *IEEE Trans. Med. Imag.*, vol. 33, no. 1, pp. 61–73, 2014.

References III



Y. Xu and W. Yin, "A block coordinate descent method for regularized multiconvex optimization with applications to nonnegative tensor factorization and completion", *SIAM J. Imag. Sci.*, vol. 6, no. 3, pp. 1758–1789, 2013.

Polychromatic X-ray CT Model via Mass Attenuation

For invertible $\kappa(\varepsilon)^{\$}$, define its inverse as $\varepsilon(\kappa)$. Then,

$$\mathcal{I}^{\text{in}} = \int \iota(\kappa) d\kappa, \quad \mathcal{I}^{\text{out}} = \int \iota(\kappa) \exp \left[-\kappa \int_{\ell} \alpha(x, y) d\ell \right] d\kappa$$

where

$$\iota(\kappa) \triangleq \iota(\varepsilon(\kappa)) |\varepsilon'(\kappa)|$$

is the **mass attenuation spectrum** and the function $\varepsilon(\kappa)$ is differentiable with derivative

$$\varepsilon'(\kappa) = \frac{d\varepsilon(\kappa)}{d\kappa}$$

◀ back

[§] Assumed for simplicity, extends easily to arbitrary $\kappa(\varepsilon)$.

Initialization and Convergence Criteria I

Initialize the density-map iterates as follows:

$$\boldsymbol{\alpha}^{(-1)} = \hat{\boldsymbol{\alpha}}_{\text{FBP}}, \quad \boldsymbol{\alpha}^{(0)} = \mathbf{0}, \quad \theta^{(0)} = 0$$

where $\hat{\boldsymbol{\alpha}}_{\text{FBP}}$ is the standard FBP reconstruction (Kak and Slaney 1988, Ch. 3).

Convergence criterion

$$\delta^{(i)} \triangleq \|\boldsymbol{\alpha}^{(i)} - \boldsymbol{\alpha}^{(i-1)}\|_2 < \epsilon \|\boldsymbol{\alpha}^{(i)}\|_2$$

where $\epsilon > 0$ is the convergence threshold.

Inner-loop convergence criteria

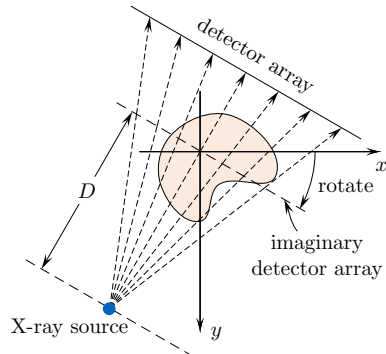
$$\begin{aligned}\|\boldsymbol{\alpha}^{(i,k)} - \boldsymbol{\alpha}^{(i,k-1)}\|_2 &< \eta_{\boldsymbol{\alpha}} \delta^{(i-1)} \\ |\mathcal{L}_A(\mathcal{I}^{(i,k)}) - \mathcal{L}_A(\mathcal{I}^{(i,k-1)})| &\leq \eta_{\mathcal{I}} \delta_{\mathcal{L}}^{(i)}\end{aligned}$$

where $\delta_{\mathcal{L}}^{(i)} = |\mathcal{L}(\boldsymbol{\alpha}^{(i)}, \mathcal{I}^{(i-1)}) - \mathcal{L}(\boldsymbol{\alpha}^{(i-1)}, \mathcal{I}^{(i-1)})|$,

- k are the inner-iteration indices, and
- the convergence tuning constants $\eta_{\boldsymbol{\alpha}} \in (0, 1)$ and $\eta_{\mathcal{I}} \in (0, 1)$ are chosen to trade off the accuracy and speed of the inner iterations and provide sufficiently accurate solutions by these iterations.

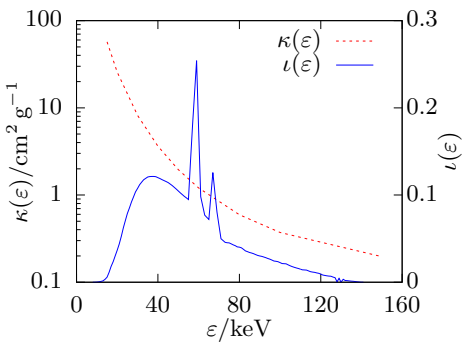
Simulated X-ray CT Example

- Equi-spaced fan-beam projections over 360° ,
- X-ray source to rotation center is $2000 \times$ detector size,
- measurement array size of 512 elements,
- image to reconstruct is of 512×512 , and
- performance metric is the relative square error (RSE) of an estimate $\hat{\alpha}$ of the signal coefficient vector:



$$\text{RSE}\{\hat{\alpha}\} = 1 - \left(\frac{\hat{\alpha}^T \alpha_{\text{true}}}{\|\hat{\alpha}\|_2 \|\alpha_{\text{true}}\|_2} \right)^2$$

Simulated X-ray CT Example



- Incident X-ray spectrum from tungsten anode X-ray tubes at 140 keV with 5 % relative voltage ripple, and
- using photon-energy discretization with 130 equi-spaced discretization points over the range 20 keV to 140 keV.

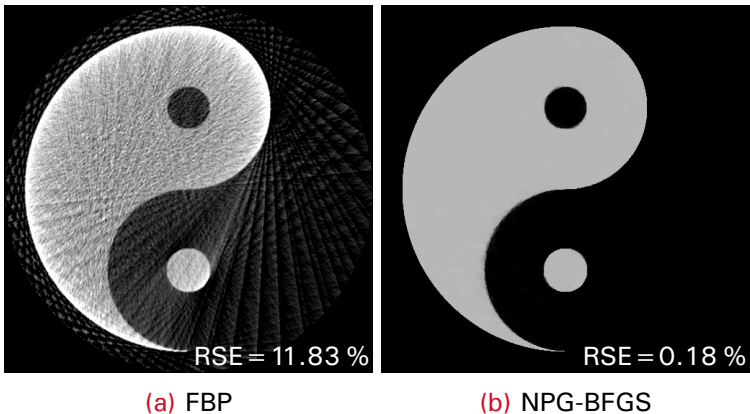


Figure 14: Reconstructions from 60 projections.

Simulated X-ray CT Example

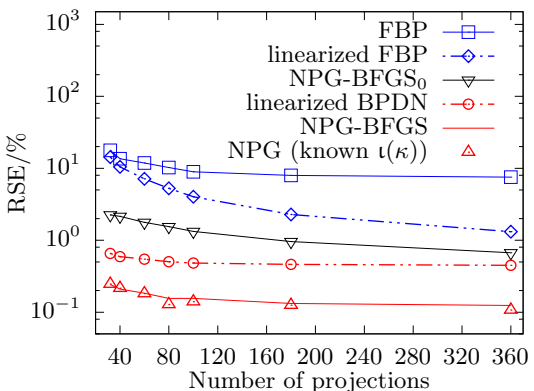


Figure 15: Average RSEs as functions of the number of projections.